IEEE Access
Multidisciplinary | Rapid Review | Open Access Journal

Received March 16, 2021, accepted March 29, 2021, date of publication April 8, 2021, date of current version April 15, 2021.

Digital Object Identifier 10.1109/ACCESS.2021.3071776

Power Decoupling Control for Single-Phase Grid-Tied PEMFC Systems With Virtual-Vector-Based MPC

WEI WANG[1], BIN LIU[1], YUKUN HU[2], (Member, IEEE), ZHOUHUA LI[1], HUI WANG[3], YANMING CHEN[1], AND SHAOJIAN SONG[1], (Member, IEEE)

[1]School of Electrical Engineering, Guangxi University, Nanning 530004, China
[2]Department of Civil, Environment and Geomatic Engineering, University College London, London WC1E 6BT, U.K.
[3]School of Automation, Central South University, Changsha 410083, China

Corresponding author: Bin Liu (bingo.liu@csu.edu.cn)

This work was supported in part by the National Natural Science Foundation of China under Grant 61863003 and Grant 61973322, and in part by the Natural Science Foundation of Hunan Province of China under Grant 2018JJ3690.

ABSTRACT The fuel cell grid-tied power generation system usually includes a dc-dc converter and a dc-ac inverter. In a single-phase system, inherent low-order current pulsations are introduced into the system, which can have harmful effects on the fuel cell stack. For example, reducing the output voltage and output efficiency, a reduction in service life, and even accelerates the degradation rate of the membrane electrode of a proton exchange membrane fuel cell (PEMFC). In addition, dc/ac coupling power can cause distortion in the dc input current and ac grid current. To eliminate the input ripple and ensure high ac power quality on the grid side, this paper proposes a novel power decoupling control for single-phase grid-tied PEMFC systems, which uses an improved model predictive control (MPC) algorithm. With the help of the virtual vector methods, which are realized by a two-stage optimization method, excellent tracking effect and robustness can be ensured. Simulations and experimental results show that the proposed algorithm can not only completely eliminate the input current ripple and reduce the total harmonic distortion (THD) of ac current on the grid side, but also improve the transient performance of the system.

INDEX TERMS Fuel cell, low frequency current ripple, model predictive control, ripple elimination.

I. INTRODUCTION

With the rapid development of portable devices, automotive applications and new energy power generation technologies [1]–[5], PEMFC has wide range of applications due to its outstanding characteristics. The main advantages of PEMFC are: 1) high power generation efficiency, 2) low environmental pollution, 3) less restrictions on installation sites, 4) low noise, 5) modular structure [6].

Given these advantages, PEMFC has also been widely used in grid-tied power generation systems [7]. However, due to the low dc voltage generated by PEMFC, a dc-dc converter is required in the fuel cell power generation system, to boost the low dc voltage to a higher voltage, and then acquires an ac voltage through the dc-ac inverter. Therefore, the fuel cell power generation system usually consists of a two-stage structure [8].

The design of fuel cell power generation system not only requires basic operating performance, but also requires high reliability, good safety performance and long service life [9]. When the fuel cell power converter is connected to the utility single-phase grid, the inherent rectification effect will cause low frequency current ripple contents on the output side of PEMFC [10]. References [11] and [12] pointed out that when the amplitude of the low frequency current ripple exceeds 4%, it will have the following adverse effects on the system: 1) make the cathode surface responses slower, 2) reduce the output capacity of the power converter, 3) deactivate the Pt electrode on the catalyst layer, 4) accelerate the degradation rate of the membrane electrode, and 5) incur nuisances such as overload situation. For these reasons, the performance and service life of the fuel cell stack and the entire system are still uncertain. Therefore, the limitation of low frequency current ripple is very important for the efficient utilization of fuel cell power generation.

Since the control strategies of low current ripple play a significant role in the reliability and durability of the power

The associate editor coordinating the review of this manuscript and approving it for publication was Chi-Seng Lam.

generation system [13], many scholars have proposed some mitigation methods of low-current ripples [14]–[18]. However, the frequency of the ripple is too low, and the passive filter has weak suppression of the inherent ripple [19]. To effectively reduce current ripple on the low-voltage dc side, various active ripple decoupling techniques using active power filter (APF) have been explored. Reference [20] proposed a concept of active-filter integration for single-phase ac/dc converters. The resultant converters can provide power factor correction, dc voltage regulation, and active power decoupling functions simultaneously to reduce low frequency dc voltage ripple. However, the APF only buffers twice of fundamental frequency power ripple, while other low frequency power ripples still exist on the dc side. Reference [21] proposed an active filtering method, which provides an alternative path for 120 Hz current to prevent it from flowing through the fuel cell. In reference [22], an energy-saving fuel cell power regulation system is optimized by using a new zero-ripple filter. The filter comprises a coupled inductor-based filter for minimizing high frequency switching ripple and an APF for mitigating low frequency ripple, thereby potentially improving the durability of the stack. However, adding additional peripheral circuits or independent energy storage devices will greatly increase the complexity and total cost of the system.

In order to reduce the number of devices and simplify the system, active control algorithms were discussed in references [23], [24] by using average filter and voltage and current dual closed-loop control method. Although, these technologies can effectively reduce low frequency ripple without adding supplementary components, due to the complexity of the voltage controller bandwidth setting and obvious overshoot, it is difficult to completely eliminate the low frequency ripple during load transients. To address this problem, reference [25] proposed an instantaneous ripple power control method based on model predictive control. It overcomes the disadvantage of poor dynamic performance during load transients. The proposed method tracks the instantaneous ripple power and can make full use of the storage capacitor. It can also achieve fast dynamics and perfectly compensate ripple power during transients or steady states. Nevertheless, when the control responds frequently, the MPC has a heavy computational load and cannot track the controlled process accurately enough. Bearing this mind, many researchers have made efforts to improve MPC algorithms in recent years. In [26], the equivalent transformation and special fan-shaped distribution method were used to reduce the calculation frequency of current prediction in a sampling period from 8 to 1, thereby reducing the computational load of current prediction and cost function. In [27], an optimal duty cycle calculation method was proposed, and a vector sequence was constructed to minimize the switching jump and obtain a better control effect. However, only a limited number of voltage vectors can be selected in traditional MPC, which will lead to inaccurate tracking and large current ripple [28]. In order to solve this problem, some scholars have proposed a method of constructing virtual vectors, which equally distributes the basic voltage vectors and increases the number of voltage vectors [29], [30]. Nevertheless, this method also involves a lot of calculations and cannot completely match the operation of the system.

Aiming at a series of drawbacks existing in the above references, a power decoupling control method for single-phase grid-tied PEMFC system based on improved model predictive control is proposed in this paper. The main contributions of this paper are as follows:

(1) The introduction of the generation and propagation mechanism of low frequency current ripple, and the configuration of the grid-tied PEMFC power generation system can eliminate current ripple without adding additional circuit.

(2) A novel power decoupling control method based on power balance technology is proposed, which can eliminate the ripple of the fuel cell current at the output and ensure the high ac power quality.

(3) The improvement of the virtual-vector-based MPC method further improves the accuracy of the virtual vector construction, and therefore can reduced the THD of the ac current on the grid side.

(4) The experimental results verify the effectiveness of the proposed power decoupling control method.

The structure of this paper is as follows: Section II introduces the model of grid-tied PEMFC power generation system and the proposed power decoupling control method; Section III details the active decoupling control algorithm with virtual-vector-based MPC; Section IV provides simulation and experimental studies, and discusses the results. Finally, Section V concludes in relation to this overall study are drawn.

II. MATHEMATICAL PROBLEM STATEMENT

A. SYSTEM CONFIGURATION OF GRID-TIED FUEL CELL GENERATION

The topology of the fuel cell grid-tied power generation system is shown in Fig.1. This system consists of a dc-dc converter and a single-phase full-bridge dc-ac inverter. The dc-dc converter is used to boost the low fuel cell voltage up to a higher value. It is composed of input capacitor C, inductor L, IGBT S_5, and diode D. The single-phase full-bridge dc-ac inverter is connected to the grid, which consists of a dc-link capacitor C_{dc} and four switches S_1-S_4. Assuming i_{FC} is the current flowing through the fuel cell, i_g is the grid current flowing through the L-type filter inductance L_f and the equivalent resistance R of line.

B. EGENERATION AND PROPAGATION MECHANISM OF COUPLING POWER

As shown in Fig. 1, the dc-ac inverter is connected in parallel with grid, thus the output voltage is exactly the same as the grid voltage. The output current of the inverter is in phase with the grid voltage. Accordingly, the instantaneous value of the output voltage and current of the dc-ac inverter can be

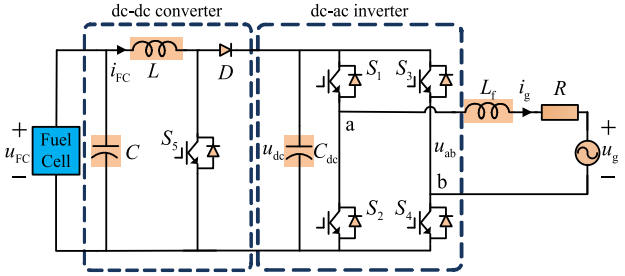

FIGURE 1. The topology of grid-tied PEMFC power generation system.

expressed respectively by (1):

$$\begin{cases} u_{\mathrm{g}}(t) = \sqrt{2}\, U_{\mathrm{m}} \sin(\omega t) \\ i_{\mathrm{g}}(t) = \sqrt{2}\, I_{m} \sin(\omega t), \end{cases} \tag{1}$$

where U_{m} and I_{m} are respectively expressed as the root mean square (rms) values, ω is the angular frequency of the grid. The instantaneous output power of the inverter can be expressed as:

$$\begin{aligned} p_{\mathrm{out}}(t) &= \sqrt{2} U_{\mathrm{m}} \sin(\omega t) \times \sqrt{2} I_{\mathrm{m}} \sin(\omega t) \\ &= U_{\mathrm{m}} I_{\mathrm{m}} [1 - \cos(2\omega t)]. \end{aligned} \tag{2}$$

It can be seen that the output power contains the fluctuation power of twice the frequency. The instantaneous output power of the PEMFC can be expressed as:

$$p_{\mathrm{FC}}(t) = u_{\mathrm{FC}}(t)\, i_{\mathrm{FC}}(t), \tag{3}$$

where, $u_{\mathrm{FC}}(t)$ and $i_{\mathrm{FC}}(t)$ are the output voltage and current of the fuel cell respectively.

Assume that there is no power loss in the system. The entire power generation system and the load satisfy the law of conservation of energy, and then the output current of the fuel cell can be obtained as:

$$i_{\mathrm{FC}}(t) = \frac{U_{\mathrm{m}} I_{\mathrm{m}} [1 - \cos(2\omega t)]}{u_{\mathrm{FC}}(t)}. \tag{4}$$

Consequently, 2ω current ripple is reflected to the fuel cell stack, which will cause harmful effects on fuel cell voltage and current.

C. PROPOSED DECOUPLING CONTROL METHOD

In this section, the proposed decoupling control method is analyzed. Conventionally, a capacitor with large capacitance is used to smooth the 2ω ripple on the output side of the dc-dc converter. However, when the energy of the 2ω ripple is high, it is hard to handle it completely only with a capacitor. Some of the 2ω ripple will still exist and even spread into the fuel cell stack. In order to mitigate the current ripple of the fuel cell, this paper proposes a novel power decoupling control for single-phase grid-tied PEMFC systems, with power balancing technique. The control block diagram is shown in Fig. 2.

With the help of the proposed control algorithm, the dc-dc converter takes charge of power control through a model predictive controller. In this controller, the current reference of the fuel cell $i_{\mathrm{FC}}{}^{*}(k)$ can be obtained by dividing the

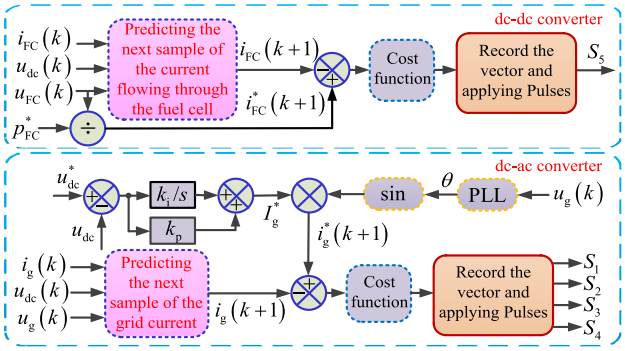

FIGURE 2. The control block diagram of the proposed power decoupling control.

constant power command $p_{\mathrm{FC}}{}^{*}$ with the measured fuel cell voltage $u_{\mathrm{FC}}(k)$. Owing to the slow decrease of $u_{\mathrm{FC}}(k)$, $i_{\mathrm{FC}}{}^{*}(k)$ is invariant during one sampling period, so $i_{\mathrm{FC}}{}^{*}(k)$ is almost equal to $i_{\mathrm{FC}}{}^{*}(k+1)$. With the good tracking performance and robustness of MPC, the fuel cell power can be controlled as constant. The output current ripple of the fuel cell can be mitigated directly.

The proposed dc-ac converter controller is consists of a dc-link voltage controller and a grid current controller, which is implemented by MPC algorithm. The dc-link voltage u_{dc} can be controlled by the power balancing technique of input and output power. The power balancing technique can be expressed as: the energy on the dc-link capacitor is proportional to the square of the voltage. Therefore, when the input energy is greater than the output energy, the dc-link voltage rises, and vice versa. It means that the energy generated by the fuel cell is transmitted to the grid in real time by using the dc-link capacitor as an energy transfer station. In other words, the output signal $I_{\mathrm{g}}{}^{*}$ of the voltage control loop is multiplied by the phase of grid to generate the reference current $i_{\mathrm{g}}^{*}(k)$ for the inverter. Since the sampling frequency is high enough, $i_{\mathrm{g}}{}^{*}(k)$ is approximately equal to $i_{\mathrm{g}}{}^{*}(k+1)$.

III. ACTIVE DECOUPLING CONTROL METHOD WITH VIRTUAL-VECTOR-BASED MPC

A. WORKING PRINCIPLE OF VIRTUAL-VECTOR-BASED MPC

The design and implementation of model predictive control includes the following three steps:

1) Building a model to predict the behavior of control variables for the next time step.
2) Construct an appropriate cost function which includes control objectives and expected behavior of the system.
3) Extract the appropriate command to minimize the cost function value.

The discrete model to predict the next step can be shown in the following equations:

$$\begin{cases} x(k+1) = ax(k) + bu(k) \\ y(k) = cx(k), \end{cases} \tag{5}$$

where $x(k)$ is the current value of the system state variables, $x(k+1)$ is the next value of $x(k)$, $u(k)$ is the current value of the system input variables, $y(k)$ is the current value of the system output variables, a is the system coefficient, b is the control coefficient, and c is the output coefficient. In next step, according to the following equation, the cost function can be obtained as:

$$J = f\left(x\left(k\right), u\left(k\right), \cdots, u\left(k+n\right)\right). \tag{6}$$

However, the application of a single switching state in traditional MPC during the whole sampling period inevitably leads to inaccurate tracking, and the performance deterioration of the converter. Owing to the limited number of voltage vectors, the accuracy of this method is compromised and higher sampling frequency is required to improve the performance. Aiming to solve this problem, this paper employs the virtual vectors and integrates them into the MPC structure to increase the number of the switching states. The virtual vectors are formulated by equally dividing the real voltage vectors V_{real} of the converters:

$$V_{\text{vir}} = \frac{m}{n} V_{\text{real}}, \tag{7}$$

where, n is the number of vectors and m varies from 1 to n.

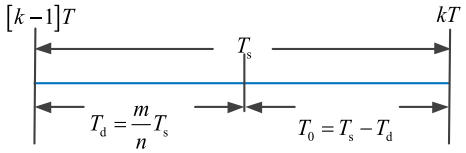

FIGURE 3. Switching period in virtual-vector-based MPC.

The construction of virtual vector increases the number of predictive values of control variables. After rolling optimization by cost function, the selected optimal vector is applied to the converter. As shown in Fig. 3, in one sampling period, the real vectors and virtual vectors are used to maintain the on-time T_{d}, and the off-time T_0 is supplemented by the zero vectors.

$$T_{\text{d}} = \frac{m}{n} T_{\text{s}}, \tag{8}$$

where T_{s} is the switching period.

B. DIRECT INPUT CURRENT RIPPLE MITIGATION CONTROL METHOD WITH VIRTUAL-VECTOR-BASED MPC FOR BOOST CONVERTER

Based on the above analysis, the output current of fuel cell i_{FC} contains 2ω ripple. To address this problem, a direct input current ripple mitigation control method with virtual-vector-based MPC is used in the boost converter.

In order to achieve a unified form of the converter under different working states, the switching function $\varepsilon(t)$ is introduced in this paper. When the switch S_5 is on, $\varepsilon(t) = 1$, and when the switch S_5 is off, $\varepsilon(t) = 0$. That is:

$$\varepsilon\left(t\right) = \begin{cases} 1 & 0 \le t < dT_{\text{s}} \\ 0 & dT_{\text{s}} \le t < T_{\text{s}}, \end{cases} \tag{9}$$

where d is the duty cycle of boost converter, it is a variable between 0 to 1.

The state equations of boost circuit can be obtained, according to the topology of dc-dc converter in Fig. 1:

$$\begin{cases} L\dfrac{\mathrm{d}i_{\text{FC}}\left(t\right)}{dt} = u_{\text{FC}}\left(t\right) & 0 \le t < dT_{\text{s}} \\ L\dfrac{\mathrm{d}i_{\text{FC}}\left(t\right)}{dt} = u_{\text{FC}}\left(t\right) - u_{\text{dc}}\left(t\right) & dT_{\text{s}} \le t < T_{\text{s}}. \end{cases} \tag{10}$$

Since the boost circuit is a time-varying nonlinear circuit, the state space average method is used to linearize the boost circuit. Equation (10) can be written in a unified form within $0 \le t < T_{\text{s}}$:

$$L\frac{\mathrm{d}i_{\text{FC}}\left(t\right)}{dt} = u_{\text{FC}}\left(t\right) - \left[1 - \varepsilon\left(t\right)\right] u_{\text{dc}}\left(t\right). \tag{11}$$

Average $\varepsilon(t)$ in a switching period:

$$\begin{aligned} \left[\varepsilon\left(t\right)\right]_{T_{\text{s}}} &= \frac{1}{T_{\text{s}}}\left(\int_0^{dT_{\text{s}}} 1\mathrm{d}t + \int_{dT_{\text{s}}}^{dT_{\text{s}}+T_{\text{s}}} 0\mathrm{d}t\right) \\ &= \frac{dT_{\text{s}}}{T_{\text{s}}} = d. \end{aligned} \tag{12}$$

Replacing $\varepsilon(t)$ with d in (11), the state space average expression can be obtained:

$$L\frac{\mathrm{d}i_{\text{FC}}\left(t\right)}{dt} = u_{\text{FC}}\left(t\right) - \left(1 - d\right) u_{\text{dc}}\left(t\right). \tag{13}$$

The forward difference of (13) is performed, the prediction equation of the output current of the fuel cell $i_{\text{FC}}(k+1)$ can be obtained:

$$i_{\text{FC}}\left(k+1\right) = i_{\text{FC}}\left(k\right) - \frac{T_{\text{s}}\left(1-d\right)u_{\text{dc}}\left(k\right)}{L} + \frac{T_{\text{s}} u_{\text{FC}}\left(k\right)}{L}. \tag{14}$$

The cost function can be created as follows:

$$J_1 = \left(i_{\text{FC}}\left(k+1\right) - i_{\text{FC}}^{*}\left(k+1\right)\right), \tag{15}$$

where, $i_{\text{FC}}{}^{*}(k+1)$ is the current reference of the fuel cell at the next moment.

The switch S_5 only has two working states in a switching period: on and off. To obtain good tracking performance, the virtual vector construction method analyzed in the previous section is adopted. The rolling optimization of the predictive current i_{FC} is shown in Fig. 4.

Through the modeling analysis above, the control block diagram of the virtual-vector-based MPC for boost converter can be given in Fig. 2. The optimal vector is selected by cost function optimization, then the duty cycle d is adjusted to control $i_{\text{FC}}(k+1)$ to track the reference current $i_{\text{FC}}{}^{*}(k+1)$. According to the analysis above in this paper, this method controls the fuel cell power to become constant. In other words, a purely constant reference value is fed into the controller, so that the 2ω current ripple can be eliminated effectively.

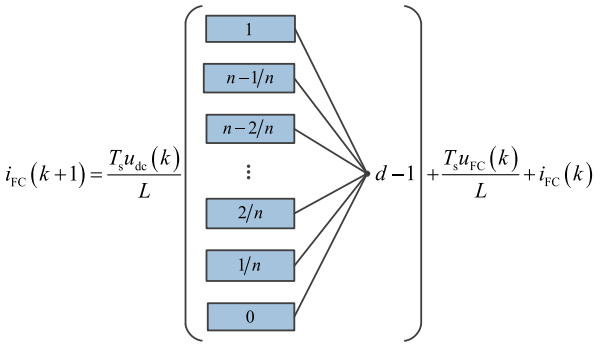

FIGURE 4. Rolling optimization of fuel cell current prediction based on virtual-vector-based MPC.

C. IMPROVED VIRTUAL-VECTOR-BASED MPC FOR THE GRID-TIED DC/AC CONTROL

This section analyzes the improved virtual-vector-based MPC for the grid-tied dc-ac inverter. The model of the inverter in Fig. 1 can be described by:

$$u_{ab}(t) = Ri_g + L_f\frac{di_g(t)}{dt} + u_g(t). \tag{16}$$

Thus, the differential of the grid current i_g can be approximately expressed as:

$$\frac{di_g(t)}{dt} \approx \frac{i_g(k+1) - i_g(k)}{T_s}. \tag{17}$$

The predicted current value at the next sampling instant, $i_g(k+1)$ can be given by substituting (17) into (16):

$$i_g(k+1) = \frac{1}{RT_s + L_f}\left[L_f i_g(k) + T_s u_{ab}(k) - T_s u_g(k)\right]. \tag{18}$$

Design the cost function can be created as follows:

$$J_2 = \left|i_g(k+1) - i_g^*(k+1)\right|, \tag{19}$$

where, $i_g{}^*(k+1)$ is the current reference of the grid at the $(k+1)$th instant.

According to the different states of the four switches $S_1 - S_4$, the inverter has only three possible output states in each switching time with traditional MPC, as shown in Fig. 5(a). A large number of the virtual states that can be constructed and utilized are ignored between 0 to u_{dc} and 0 to $-u_{dc}$. This will lead to much harmonics in the grid current i_g.

When the virtual-vector-based MPC which analyzed in section A is adopted in the inverter, the number of the voltage vector will be increased, as shown in Fig. 5(b), these vectors include four real vectors (the circle symbols in red) and several constructed virtual vectors (the square symbols in black).

Obviously, the larger the n, the better tracking performance of the grid current i_g, but the computational load will also increase. The huge amount of calculation increases the computational load of the digital signal processor (DSP). Therefore, it is only a theoretically possible to find a perfect virtual vector for every actual value in the whole control

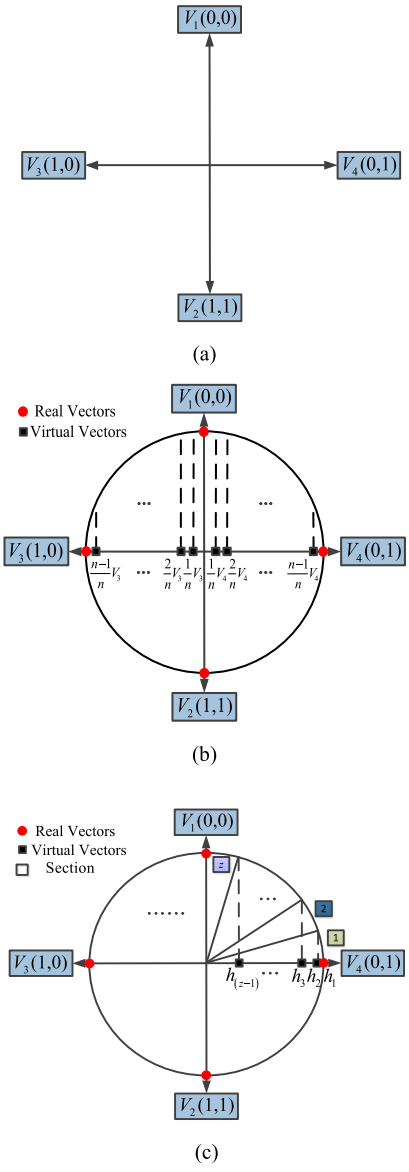

FIGURE 5. Voltage vectors generated by the single-phase inverter. (a) With the traditional MPC. (b) With the virtual-vector-based MPC. (c) With the improved virtual-vector-based MPC.

space. For meeting the computing load, and make it feasible to implement by a digital microcontroller unit, the number of vectors n, cannot be too high, there will be non-ignorable error between the actual operation of the system and the virtual vector. As the ideal grid voltage and current converted to the $\alpha\beta$ axis of the two-phase static coordinate system is a vector circle rotating at angular frequency ω, the control target of the grid-tied inverter is to approach this circle infinitely. Therefore, this paper proposes an improved method of constructing virtual vector, with two steps. Initially, the sector information of the ideal grid voltage and current is used for the preselection of the reference vector. After the calculation of the reference vector for the first step, the improved virtual vectors are constructed in the second step. Finally, the optimal vector is selected by the cost function. This method is more

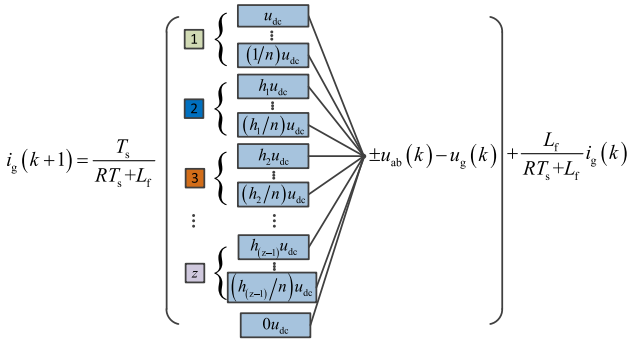

FIGURE 6. Rolling optimization of inverter output current prediction based on improved virtual-vector-based MPC.

in line with the actual operation of the system, while reducing the amount of calculation.

The improved method of constructing virtual vector can be described as two parts:

1) Calculate reference vectors: dividing the vector circle into z sectors equally, and then calculates the cosine value corresponding to radian angle of each sector.
2) Construct the improved virtual vectors: dividing the vector reference of each sector into n parts equally.

Taking a quarter cycles as an example, divide a quarter vector circles into z sectors as shown in the Fig. 5(c). Where h_i is the reference vector corresponding to different sectors. It can be expressed as:

$$h_i = \cos\left[\left(\frac{90^o}{z}\right)(i-1)\right], \tag{20}$$

where i is an integer between 1 to z.

Therefore, the improved virtual vector $V_{hi,m}$ can be obtained by dividing the reference vector h_i equally within each sector:

$$V_{h_i,m} = \begin{cases} \frac{m}{n}h_i V_4 \\ \frac{m}{n}h_i V_3, \end{cases} \tag{21}$$

where m is an integer between 1 to n.

The vectors in Fig. 5(c) include four real vectors (the circle symbols in red) and several constructed virtual vectors (the square symbols in black).

In the improved virtual-vector-based MPC, the output inverter voltage can be given as:

$$u_{ab} = \pm\frac{m}{n}h_i u_{dc}. \tag{22}$$

The predictive current process of rolling optimization is shown in Fig. 6. All the states of u_{ab} in (22) will be placed in (18) and $i_g(k+1)$ can be calculated. Then, $i_g(k+1)$ is substituted in the cost function J_2. The amount of $i_g(k+1)$, which minimizes the cost function, determines the reference voltage $u_{ab}{}^*$ of the inverter. The duty cycle can be obtained as:

$$T_d = \frac{u_{ab}^*}{u_{dc}}T_s, \quad \text{or,} \quad T_d = \frac{m}{n}h_i T_s. \tag{23}$$

TABLE 1. Switching table for applying vectors in the proposed virtual-vector-based MPC.

Detected sectors	Selected vector	T_s	
		T_d	T_0
Sector 1	$V_{3,m}$	$(m/n)V_3(1,0)$	
	$V_{4,m}$	$(m/n)V_4(1,0)$	
Sector 2	$V_{h_1,m}$	$(m/n)V_{h_1}(h_1,0)$	
	$V_{-h_1,m}$	$(m/n)V_{-h_1}(0,h_1)$	$V_1(0,0)$ $V_2(1,1)$
Sector 3	$V_{h_2,m}$	$(m/n)V_{h_2}(h_2,0)$	
	$V_{-h_2,m}$	$(m/n)V_{-h_2}(0,h_2)$	
…	…	…	
Sector z	$V_{h_{(z-1)},m}$	$(m/n)V_{h_{(z-1)}}(h_{(z-1)},0)$	
	$V_{-h_{(z-1)},m}$	$(m/n)V_{-h_{(z-1)}}(0,h_{(z-1)})$	

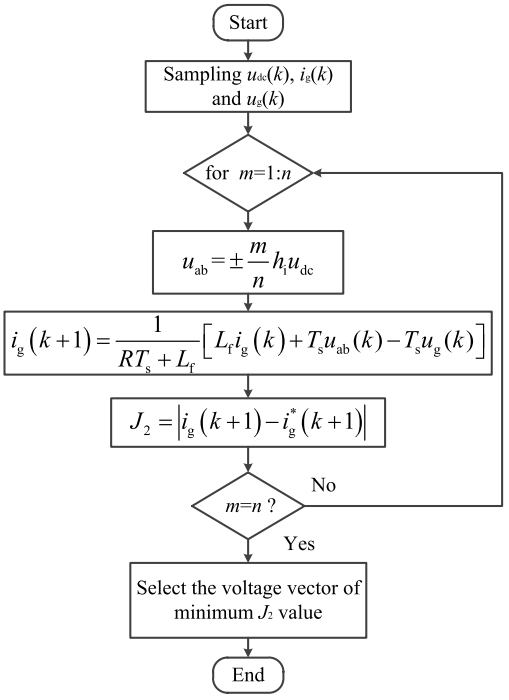

FIGURE 7. The control flow chart of the improved virtual-vector-based MPC.

After the determination of the inverter voltage reference $u_{ab}{}^*$, this vector will be applied by switching table shown in Table 1. In this case, the optimal vector selected by the cost function is applied during T_d, and then the rest of the switching time T_0 is compensated by the zero vector (V_1, V_2), where:

$$T_0 = T_s - T_d. \tag{24}$$

The control flow chart of the improved virtual-vector-based MPC is shown in Fig. 7.

The control block diagram of single-phase grid-tied dc-ac inverter is shown in Fig. 2. This control method adjusts the dc-link voltage and controls the output current at the

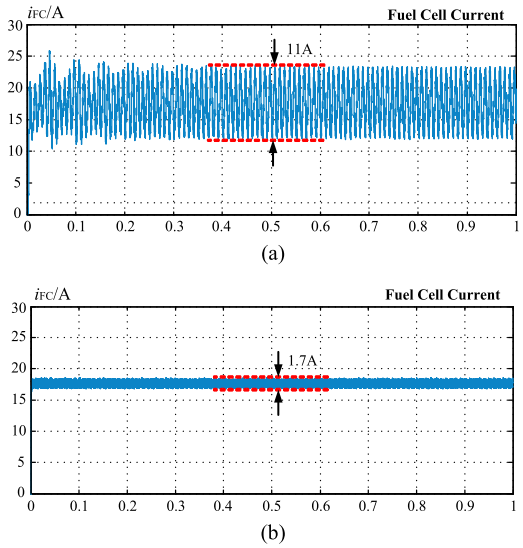

FIGURE 8. Simulation results of fuel cell current at steady-state. (a) With traditional PI control. (b) With virtual-vector-based MPC.

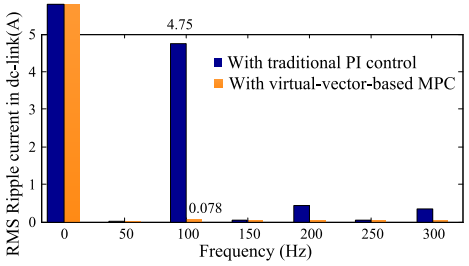

FIGURE 9. The FFT analysis of fuel cell current.

TABLE 2. Parameters for simulation.

Parameters	Symbols	Values	Unit
Input voltage	u_{FC}	85	V
dc-link voltage	u_{dc}	180	V
Grid voltage	u_g	110	V
Frequency of the grid	f	50	Hz
Input capacitor	C	20	μF
dc-link capacitor	C_{dc}	200	μF
dc-link inductor	L	2	mH
Filter inductance	L_f	2	mH
Filter leakage resistance	R	0.001	Ω

same time. The MPC algorithm based on virtual vector is reasonably improved to enhance the tracking effect, and it has high accuracy but without much computational demand. This will cause a good performance in terms of THD.

IV. SIMULATION AND EXPERIMENTAL RESULTS

A. SIMULATION RESULTS

To verify the efficacy of the proposed method, simulation has been carried out in the MATLAB-Simulink environment. The parameters used in the simulations are presented in Table 2. Fig. 8 shows the steady-state analysis of the boost circuit in the grid-tied PEMFC power generation system. As shown in Fig. 8(a), when PI controller is used, it can be seen that the fuel cell current has a large ripple, 11A

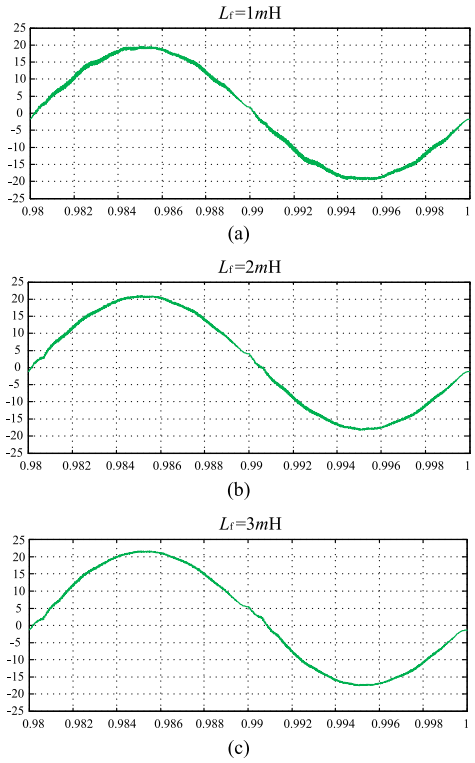

FIGURE 10. Grid current by the improved virtual-vector-based MPC in various grid impedance condition. (a) $L = 1mH$. (b) $L = 2mH$. (c) $L = 3mH$.

(peak-peak value) is observed. When the virtual-vector-based MPC is adopted, the 2ω fuel cell output current ripple can be effectively mitigated, as shown in Fig. 8(b). The current ripple can be mitigated from 11A to 1.7A (peak-peak value). Fig. 9 shows the fast Fourier transform (FFT) analysis results under the two control methods. When traditional PI control is adopted, the amplitude of the 2ω current ripple reaches 4.75A. However, with the virtual-vector-based MPC, the 2ω ripple decreased from 4.75A to 0.078A. This result effectively shows the 2ω current ripple on the dc side is significantly inhibited.

The proposed control method is based on a switching table in Table 1, where the algorithm searches the best voltage vector to track the current reference. Therefore, the change of inductor L_f has little effect on the proposed controller. As the predictive control of the current is carried out in this paper, the system parameter capacitance C does not affect the predictive control process when the model is established, and the resistance R is so small that it can be ignored. So we only carry out simulation analysis on the change of the inverter output current i_g when the inductance L_f changes. Fig. 10 shows the comparison of grid current when the grid impedance changes from $1mH$ to $3mH$. It can be seen that the proposed MPC controller is robust against the variation and keeps the grid current stable. Meanwhile, the change of grid impedance does not bring obvious oscillation.

The transient responses to load step change from 1500W to 3000W are plotted in Fig. 11 and Fig. 12 under identical conditions with the simulation results in Fig. 8. In the

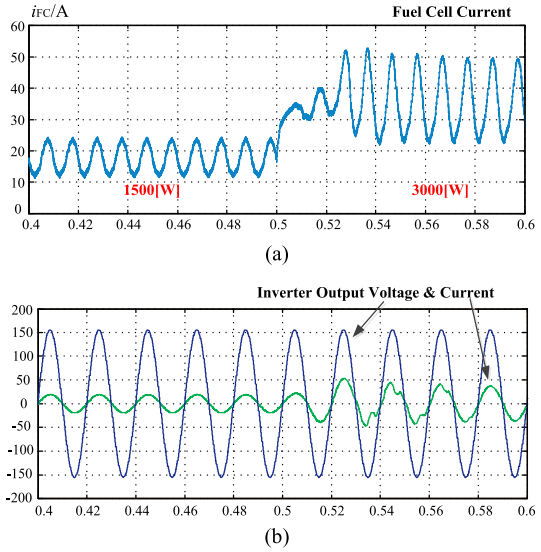

FIGURE 11. Step response at transient-state of traditional PI control. (a) Fuel cell current. (b) Inverter output voltage and current.

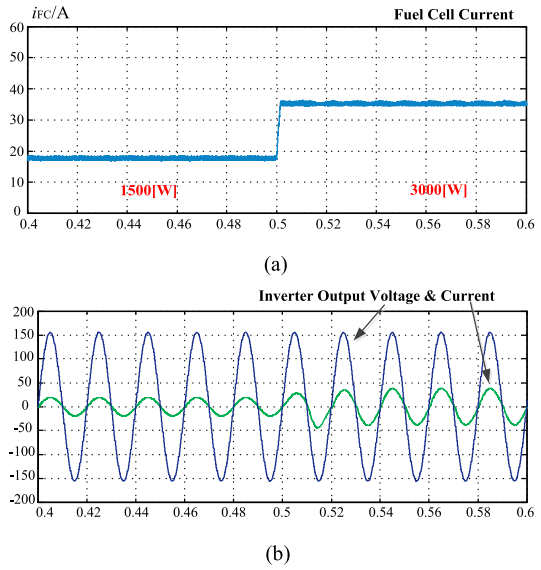

FIGURE 12. Step response at transient-state of virtual-vector-based MPC. (a) Fuel cell current. (b) Inverter output voltage and current.

case of using the PI control, there is a huge overshoot of approximately 45% and the settling time is 40ms, as shown in Fig. 11(a). However, when using the virtual-vector-based MPC, the transient response is greatly improved. As a result, the overshoot is suppressed to 4%, as shown in Fig. 12(a), only 1.5ms settling time is needed.

Under the same condition, the simulation results of traditional MPC, virtual-vector-based MPC and improved virtual-vector-based MPC are compared. The waveforms of dc-link voltage, the inverter output current and grid voltage are shown in Fig. 13. As shown in Fig. 13(a), when traditional MPC is used, the output current waveform of inverter is seriously distorted, which cannot meet the requirements of power quality. However, as shown in Fig. 13(b) and Fig. 13(c), the waveforms show that the quality of the inverter output

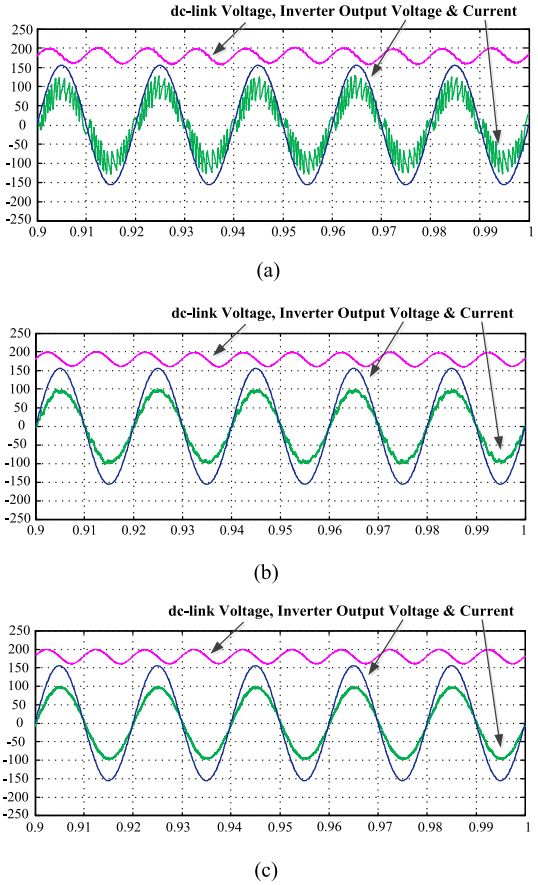

FIGURE 13. Simulation results of dc-link voltage and inverter output voltage and current. (a) With traditional MPC. (b) With virtual-vector-based MPC. (c) With improved virtual-vector-based MPC.

current is continuously improved, when the improvement of MPC is adopted. Obviously, with the improved virtual-vector-based MPC, the quality of the grid current is improved to meet the requirement of grid-connected standards. For easy comparison, the inverter current scale is magnified by 5 times as the original value.

The THD of the output current under the three methods are compared through the FFT analysis. With traditional MPC, 18.09% of THD in the grid current has been measured, as shown in Fig. 14. When the virtual-vector-based MPC is adopted, its THD decreased to 3.98%, and when the improved virtual-vector-based MPC is adopted, only 2.59% of THD has been measured. It is easy to see that the proposed method in this paper effectively reduces the THD.

B. EXPERIMENTAL RESULTS

To verify the theoretical analysis, an experimental prototype of a fuel cell power generation system with a rated power of 1.5kVA is built and tested, with 20kHz sampling frequency and switching frequency, as shown in Fig. 15. A Chroma programmable dc source simulator (62150H) is used, with the I-V Current Edit function, for the fuel cell imitating. L_f is $2mH$, the capacitance of the dc-link capacitor C_{dc} is $200\mu F$. The parameters of the prototype are shown in Table 3.

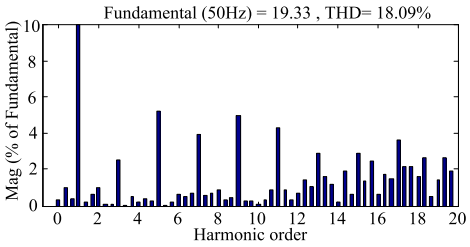

(a)

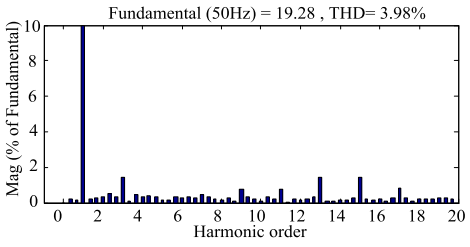

(b)

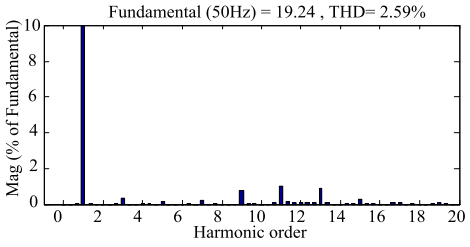

(c)

FIGURE 14. FFT analysis results of output current. (a) With traditional MPC. (b) With virtual-vector-based MPC. (c) With improved virtual-vector-based MPC.

TABLE 3. Parameters of the prototype.

Parameters	Symbols	Values	Unit
Fuel cell voltage	u_{FC}	75~92	V
Bus voltage	u_{dc}	180	V
Grid voltage	u_g	110	V
Sampling frequency	f_s	20	kHz
Switching frequency	f	20	kHz
dc-link capacitor	C_{dc}	200	μF
Filter inductance	L_f	2	mH
Filter leakage resistance	R	0.001	Ω

The control algorithm of the converter is realized on a universal control board (digital signal processor TMS320F28335 and CPLD XC9536XL).

The steady-state experimental waveforms are shown in Fig. 16. In this working state, the grid current i_g is sinusoidal and in phase with the grid voltage u_g. Fig. 16(a) shows the experimental results of using the traditional PI algorithm at rated power, the 6.2A (peak-peak value) current ripple of the fuel cell current i_{FC} is measured in the input side. On the other hand, Fig. 16(b) shows the ripple of the fuel cell current is suppressed by the proposed improved MPC method. The low frequency current ripple, especially the 2ω ripple, is approximately eliminated to zero, which effectively

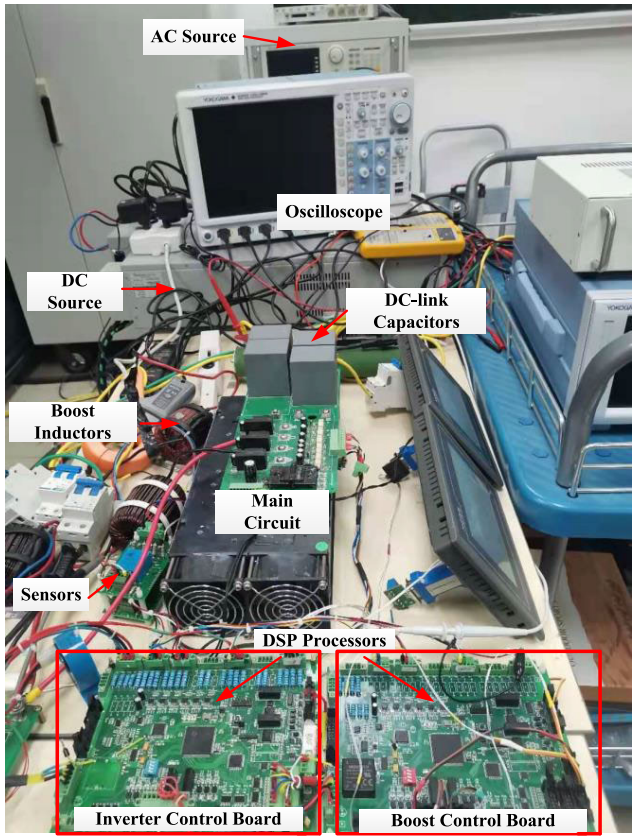

FIGURE 15. The hardware prototype picture.

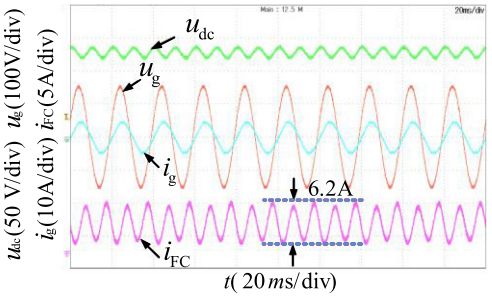

(a)

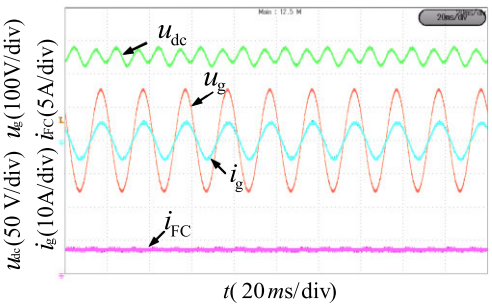

(b)

FIGURE 16. Experimental results at steady-state. (a) With traditional PI control. (b) With the proposed improved MPC.

solves the adverse effect of excessive current ripple on the fuel cell. In order to observe the change of the fuel cell voltage

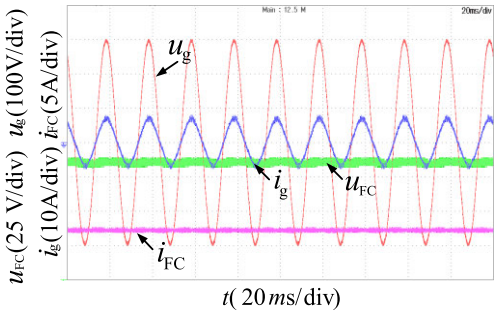

FIGURE 17. Experimental results for the proposed improved MPC within fuel cell voltage u_{FC}.

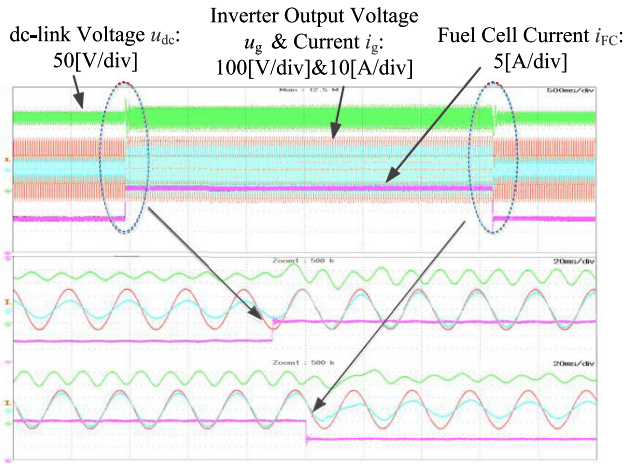

FIGURE 18. Experimental results at transient-condition.

more intuitively, the waveform of the fuel cell voltage u_{FC} is shown in Fig. 17.

It is noticed that, since the studied prototype in this paper has no energy storage element, the oscillation energy at 2ω will still exist in the system. Therefore, while the low frequency current ripple on the dc side is eliminated, the coupled power ripple is transferred from the fuel cell current to the dc-link voltage, and there is an increase in the voltage ripple, which will bring some drawbacks to the system. First, it may cause the instability in the system. Second, it may increase the distortion of output current, which will affect the output power quality. As the improved virtual-vector-based MPC method is adopted in this paper, the drawbacks above can be effectively addressed. The dynamic response of the system and the output power quality can be improved, and meet the requirement of grid-connected standards.

In addition, the decoupling control method proposed in this paper was used to analyze the abnormal step response when the power changes sharply from 1000W to 2000W, as shown in Fig. 18, overshoot and undershoot occur during the rise and fall of the transient load, respectively. The settling time under step-up and step-down conditions is within one fundamental frequency cycle. With the proposed control algorithm of the boost circuit, the transient response of the system is very fast and robust. In addition, even if the load step changes suddenly (such as an abnormal situation), the proposed scheme

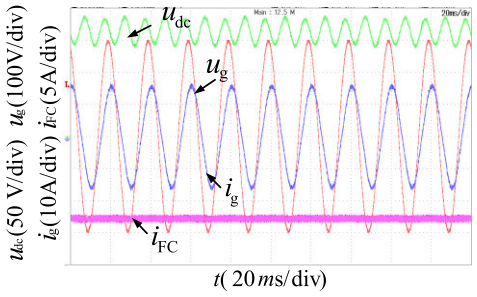

(a)

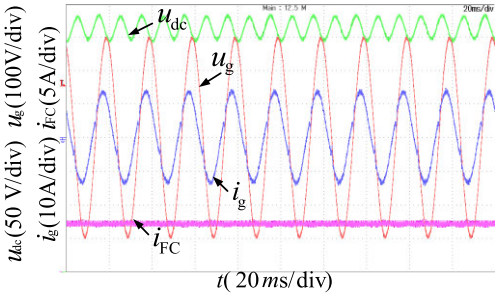

(b)

FIGURE 19. Experimental results for different power factor with the proposed improved MPC. (a) cos$\varphi = 0.95$. (b) cos$\varphi = -0.95$.

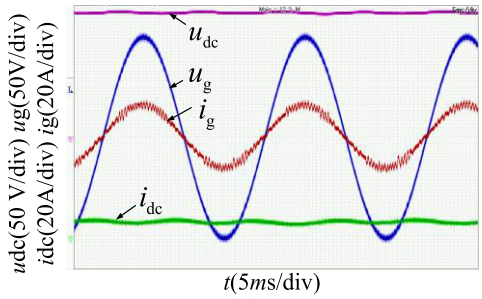

(a)

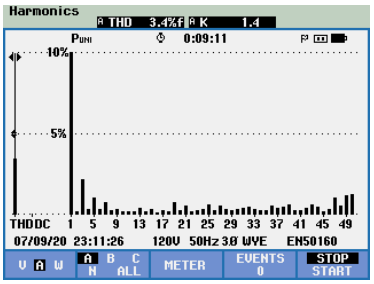

(b)

FIGURE 20. Experimental results of virtual-vector-based MPC. (a) Waveform of grid voltage and current. (b) THD.

can effectively eliminate the 2ω current ripple. Experimental results are in good agreement with the simulation results.

In order to further illustrate the feasibility of the decoupling control method proposed in this paper, the experimental results of different power factors are given. According to the new international standards for grid-connected distributed generation system, when the power level is between 3.68kVA and 13.8kVA, the commended power factor of a

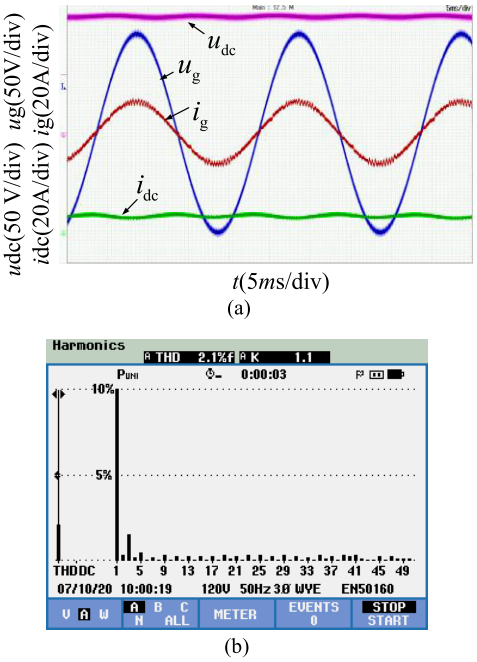

FIGURE 21. Experimental results of improved virtual-vector-based MPC. (a) Waveform of grid voltage and current. (b) THD.

grid-connected inverter is from 0.95 leading to 0.95 lagging [31]. Furthermore, reactive power should be provided to the power grid to improve the power quality of the grid. As shown in Fig. 19(a), it can be seen that the grid current i_g lays grid voltage u_g, with power factor $\cos\varphi = 0.95$. As shown in Fig. 19(b), the grid current i_g is ahead of the grid voltage u_g, with $\cos\varphi = -0.95$. Where, φ is the phase angle between grid voltage and current. It can be clearly seen from the experimental waveforms that the low frequency current ripple on the fuel cell current i_{FC} is effectively suppressed in the above two cases.

Fig. 20 shows the waveforms of grid voltage and current when a traditional MPC is used in a dc-ac inverter. The THD of the grid current i_g is 3.4%. In addition, the improved virtual-vector-based MPC method proposed in this paper improves the ac output power quality. The THD of the grid current i_g is reduced from 3.4% to 2.1%, as shown in Fig. 21.

V. CONCLUSION

This paper proposes a novel power decoupling control for single-phase grid-tied PEMFC systems, which uses an improved model predictive control algorithm. This method can reduce the input ripple without extra hardware and cost, it has outstanding performance at steady-state as well as a transient-state. In application, due to the limited number of voltage vectors in the traditional MPC method, it will bring about defects such as inaccurate tracking, large ripple and high THD. This paper proposes an improved virtual vectors construction method, with two-step optimization. This method can ensure high dc and ac power quality. The experimental results verified the reliability of the proposed algorithm.

In real world, since the converter operates different from its ideal theoretical condition, we will add an observer to the MPC controller in the subsequent work to operate the MPC through online measurement of the output power, so as to achieve better control accuracy.

REFERENCES

[1] H. Lund, "Renewable energy strategies for sustainable development," *Energy*, vol. 32, no. 6, pp. 912–919, Jun. 2007.
[2] Y. Cao and J. AbuQahouq, "Hierarchical SOC balancing controller for battery energy storage system," *IEEE Trans. Ind. Electron.*, early access, Sep. 10, 2020, doi: 10.1109/TIE.2020.3021608.
[3] J. Aghaei and M.-I. Alizadeh, "Demand response in smart electricity grids equipped with renewable energy sources: A review," *Renew. Sustain. Energy Rev.*, vol. 18, pp. 64–72, Feb. 2013.
[4] S. D. Uwe, M. Kleimaier, and W. Glaunsinger, "Relevance of energy storage in future distribution networks with high penetration of renewable energy sources," in *Proc. 20th Int. Conf. Electr. Distrib. Exhib.*, vol. 1, Jun. 2009, pp. 1–4.
[5] H. Li, K. Zhang, H. Zhao, S. Fan, and J. Xiong, "Active power decoupling for high-power single-phase PWM rectifiers," *IEEE Trans. Power Electron.*, vol. 28, no. 3, pp. 1308–1319, Mar. 2013.
[6] C. J. Hatziadoniu, A. A. Lobo, F. Pourboghrat, and M. Daneshdoost, "A simplified dynamic model of grid-connected fuel-cell generators," *IEEE Trans. Power Del.*, vol. 17, no. 2, pp. 467–473, Apr. 2002.
[7] T. P. Kumar, Y. Chandrashekar, N. Subrahmanyam, and M. Sydulu, "Control strategies of a fuzzy controlled grid connected hybrid PV/PEMFC/battery distributed generation system," in *Proc. Power Energy Conf. Illinois (PECI)*, vol. 1, Feb. 2015, pp. 1–6.
[8] E. Santi, D. Franzoni, A. Monti, D. Patterson, F. Ponci, and N. Barry, "A fuel cell based domestic uninterruptible power supply," in *Proc. 17th Annu. IEEE Appl. Power Electron. Conf. Expo. (APEC)*, vol. 1, Mar. 2002, pp. 605–613.
[9] S. Jain, J. Jiang, X. Huang, and S. Stevandic, "Modeling of fuel-cell-based power supply system for grid interface," *IEEE Trans. Ind. Appl.*, vol. 48, no. 4, pp. 1142–1153, Aug. 2012.
[10] W. Choi, G. Joung, P. N. Enjeti, and J. W. Howze, "An experimental evaluation of the effects of ripple current generated by the power conditioning stage on a proton exchange membrane fuel cell stack," *J. Mater. Eng. Perform.*, vol. 13, no. 3, pp. 257–264, Jun. 2004.
[11] R. S. Gemmen, "Analysis for the effect of inverter ripple current on fuel cell operating condition," *J. Fluids Eng.*, vol. 125, no. 3, pp. 576–585, May 2003.
[12] W. Choi, P. N. Enjeti, and J. W. Howze, "Development of an equivalent circuit model of a fuel cell to evaluate the effects of inverter ripple current," in *Proc. 19th Annu. IEEE Appl. Power Electron. Conf. Expo. (APEC)*, Feb. 2004, pp. 355–361.
[13] Y. Zhan, Y. Guo, J. Zhu, L. Li, B. Yang, and B. Liang, "A review on mitigation technologies of low frequency current ripple injected into fuel cell and a case study," *Int. J. Hydrogen Energy*, vol. 45, no. 46, pp. 25167–25190, Sep. 2020.
[14] D. Sha, Y. Xu, J. Zhang, and Y. Yan, "Current-fed hybrid dual active bridge DC–DC converter for a fuel cell power conditioning system with reduced input current ripple," *IEEE Trans. Ind. Electron.*, vol. 64, no. 8, pp. 6628–6638, Aug. 2017.
[15] N. Lu, S. Yang, and Y. Tang, "Ripple current reduction for fuel-cell-powered single-phase uninterruptible power supplies," *IEEE Trans. Ind. Electron.*, vol. 64, no. 8, pp. 6607–6617, Aug. 2017.
[16] H. Ramirez-Murillo, C. Restrepo, T. Konjedic, J. Calvente, A. Romero, C. R. Baier, and R. Giral, "An efficiency comparison of fuel-cell hybrid systems based on the versatile buck–boost converter," *IEEE Trans. Power Electron.*, vol. 33, no. 2, pp. 1237–1246, Feb. 2018.
[17] Y. Shi, B. Liu, and S. Duan, "Low-frequency input current ripple reduction based on load current feedforward in a two-stage single-phase inverter," *IEEE Trans. Power Electron.*, vol. 31, no. 11, pp. 7972–7985, Nov. 2016.
[18] R. Wang, F. Wang, D. Boroyevich, and P. Ning, "A high power density single phase PWM rectifier with active ripple energy storage," in *Proc. IEEE Appl. Power Electron. Conf.*, Feb. 2010, pp. 1378–1383.
[19] J.-S. Kim, G.-Y. Choe, H.-S. Kang, and B.-K. Lee, "Robust low frequency current ripple elimination algorithm for grid-connected fuel cell systems with power balancing technique," *Renew. Energy*, vol. 36, no. 5, pp. 1392–1400, May 2011.

[20] S. Li, W. Qi, S.-C. Tan, and S. Y. Hui, "Integration of an active filter and a single-phase AC/DC converter with reduced capacitance requirement and component count," *IEEE Trans. Power Electron.*, vol. 31, no. 6, pp. 4121–4137, Jun. 2016.
[21] W. Shireen and H. R. Nene, "Input ripple current compensation using DSP control in reliable fuel cell power systems," *Int. J. Hydrogen Energy*, vol. 37, no. 9, pp. 7807–7813, May 2012.
[22] S. K. Mazumder, R. K. Burra, and K. Acharya, "A ripple-mitigating and energy-efficient fuel cell power-conditioning system," *IEEE Trans. Power Electron.*, vol. 22, no. 4, pp. 1437–1452, Jul. 2007.
[23] Y. Song, S. B. Han, X. Li, S. I. Park, H. G. Jeong, and B. M. Jung, "A power control scheme to improve the performance of a fuel cell hybrid power," in *Proc. IEEE Power Electron. Spec. Conf.*, Jun. 2007, pp. 1261–1266.
[24] C. Liu and J.-S. Lai, "Low frequency current ripple reduction technique with active control in a fuel cell power system with inverter load," *IEEE Trans. Power Electron.*, vol. 22, no. 4, pp. 1429–1436, Jul. 2007.
[25] B. Ge, X. Li, H. Zhang, Y. Liu, R. S. Balog, H. Abu-Rub, and L. Alpuerto, "Direct instantaneous ripple power predictive control for active ripple decoupling of single-phase inverter," *IEEE Trans. Ind. Electron.*, vol. 65, no. 4, pp. 3165–3175, Apr. 2018.
[26] C. Xia, T. Liu, T. Shi, and Z. Song, "A simplified finite-control-set model-predictive control for power converters," *IEEE Trans. Ind. Informat.*, vol. 10, no. 2, pp. 991–1002, May 2014.
[27] Y. Zhang, W. Xie, Z. Li, and Y. Zhang, "Model predictive direct power control of a PWM rectifier with duty cycle optimization," *IEEE Trans. Power Electron.*, vol. 28, no. 11, pp. 5343–5351, Nov. 2013.
[28] K. S. Alam, D. Xiao, M. P. Akter, D. Zhang, J. Fletcher, and M. F. Rahman, "Modified MPC with extended VVs for grid-connected rectifier," *IET Power Electron.*, vol. 11, no. 12, pp. 1926–1936, May 2018.
[29] E. Z. Bighash, S. M. Sadeghzadeh, E. Ebrahimzadeh, Y. Yang, and F. Blaabjerg, "A novel model predictive control for single-phase grid-connected photovoltaic inverters," in *Proc. IEEE Energy Convers. Congr. Expo. (ECCE)*, Oct. 2017, pp. 461–467.
[30] E. Z. Bighash, S. M. Sadeghzadeh, E. Ebrahimzadeh, and F. Blaabjerg, "Adaptive-harmonic compensation in residential distribution grid by rooftop PV systems," *IEEE J. Emerg. Sel. Topics Power Electron.*, vol. 6, no. 4, pp. 2098–2108, Dec. 2018.
[31] B. Liu, M. Su, J. Yang, D. Song, D. He, and S. Song, "Combined reactive power injection modulation and grid current distortion improvement approach for H6 transformer-less photovoltaic inverter," *IEEE Trans. Energy Convers.*, vol. 32, no. 4, pp. 1456–1467, Dec. 2017.

WEI WANG received the B.S. degree in electrical engineering and the automation from the Lanzhou University of Technology of China, Lanzhou, China, in 2018. He is currently pursuing the M.S. degree in electrical engineering with Guangxi University, Nanning, China. His research interests include the power electronics and energy conversion, particular emphasis on converter modeling and control.

BIN LIU received the Ph.D. degree from the School of Information Science and Engineering, Central South University, Changsha, China, in 2014. Since 2015, he has been an Associate Professor with the School of Electrical Engineering, Guangxi University. His research interests include power electronics and energy conversion, with particular emphasis on converter topologies, modeling, and control.

YUKUN HU (Member, IEEE) received the Ph.D. degree in chemical engineering from the Royal Institute of Technology (KTH), Sweden, in February 2013. He is currently an Associate Professor of infrastructure systems with the Department of Civil, Environment and Geomatics Engineering, University College London (UCL) and a member of the UCL's Infrastructure Systems Institute, where he leads the energy theme research. His research interests include development of advanced modeling, control, and optimisation methods in the field of energy processes. He has experience in a wide range of modeling methods such as molecular dynamics, process simulation, computational fluid dynamics (CFD), zone modeling, agent-based modeling, and artificial intelligence techniques, including neural networks and genetic algorithms.

ZHOUHUA LI received the B.S. degree in electrical engineering and automation from the Changchun University of Science and Technology, Changchun, China, in 2019. He is currently pursuing the M.S. degree in power electronics and drives with Guangxi University, Nanning, China. His research interests include converter modeling and control techniques for distributed systems, and power quality.

HUI WANG received the B.S., M.S., and Ph.D. degrees from Central South University, Changsha, China, in 2008, 2011, and 2014, respectively. Since 2016, he has been with the School of Automation, Central South University. His research interests include matrix converter, DC/DC converters, and solid-state transformer.

YANMING CHEN received the Ph.D. degree from the South China University of Technology, Guangzhou, China, in 1998. Since 2006, he has been a Full Professor with the School of Electrical Engineering, Guangxi University. His current research interests include high-efficiency power electronics conversions for high power and energy applications.

SHAOJIAN SONG (Member, IEEE) received the B.S. degree in industrial electrical automation and the M.S. degree in control theory and control engineering from Guangxi University, Nanning, China, in 1994 and 2001, respectively. He is currently a Professor with the School of Electrical Engineering, Guangxi University. His current research interests include modeling, optimization and control for complex systems, electric vehicle, and V2G.